C. R. Acad. Sci. Paris, t. 2, Série IV, p. 1271–1286, 2001
Relativité, gravitation/*Relativity, gravitation*
(Métrologie, instrumentation/*Metrology, instrumentation*)

MISSIONS SPATIALES EN PHYSIQUE FONDAMENTALE
SPACE MISSIONS FOR FUNDAMENTAL PHYSICS

MICROSCOPE, testing the equivalence principle in space

Pierre TOUBOUL [a], Manuel RODRIGUES [a], Gilles MÉTRIS [b], Bernard TATRY [c]

[a] **ONERA, BP 72, 92322 Châtillon, France**

[b] **OCA, avenue Nicolas-Copernic, 06130 Grasse, France**

[c] **CNES, Bpi 2220, 18, avenue Edouard-Belin, 31401 Toulouse cedex 4, France**
E-mail: touboul@onera.fr; mrodrig@onera.fr; metris@obs-azur.fr; bernard.tatry@cnes.fr

(Reçu le 18 juillet 2001, accepté le 29 juillet 2001)

Abstract. The test of the equivalence principle can be performed in space with orders of magnitude better resolution than in the laboratory, because of the outstanding steady and soft environment of the in-orbit experiment. The expected new experimental results will contribute to the unification of the four interactions, demonstrate the existence of extra scalar interaction or participate in the research for a quantum gravity theory. The MICROSCOPE space mission is being developed within the framework of the Cnes scientific program with the objective of testing the universality of free fall with a 10^{-15} accuracy. The concept and the design of the experiment are discussed and the major performance drivers of the room temperature instrument are pointed out. The launch of the drag-free satellite is scheduled for late 2004. By its specific technology demonstration, the mission will open the way to even more accurate acceleration measurements for other space missions in fundamental physics. © 2001 Académie des sciences/Éditions scientifiques et médicales Elsevier SAS

MICROSCOPE / equivalence principle / electrostatic accelerometer / drag-free satellite

MICROSCOPE, test du principe d'équivalence dans l'espace

Résumé. *Réaliser le test du principe d'équivalence en orbite à bord d'un satellite dédié devrait permettre de gagner plusieurs ordres de grandeur sur la précision obtenue aujourd'hui dans les expériences de laboratoire. Une telle expérience spatiale contribuera aux efforts de grande unification des interactions, à la recherche d'une nouvelle interaction ou aux tentatives de théories de gravité quantique. La mission MICROSCOPE est en cours de développement au sein des programmes scientifiques du CNES, elle a pour objectif de tester l'universalité de la chute des corps avec une précision de* 10^{-15}. *Le principe et la configuration de l'expérience sont discutés. La précision de l'instrumentation qui fonctionne à température ambiante est détaillée. Le lancement du satellite à traînée compensée est programmé pour la fin de l'année* 2004. *Par la démonstration des nouvelles techniques spatiales qu'elle requiert, cette mission devrait ouvrir la voie à des missions spatiales encore plus ambitieuses dans le domaine de la physique fondamentale © 2001 Académie des sciences/Éditions scientifiques et médicales Elsevier SAS*

MICROSCOPE / principe d'équivalence / accéléromètre électrostatique / satellite à traînée compensée

Note présentée par Pierre ENCRENAZ.

S1296-2147(01)01264-1/FLA

Version française abrégée

De nombreuses expériences de laboratoire ont été réalisées afin de tester le principe d'équivalence avec une précision toujours accrue. Ces expériences visent d'une part à consolider la théorie de la relativité générale, d'autre part à compléter notre connaissance expérimentale en vue de la recherche d'une nouvelle interaction prédite par les tentatives théoriques de grande unification. Des résultats récents ont été obtenus au moyen de pendules de torsion supportant des masses d'épreuve constituées de matériaux différents entraînées dans le champ gravitationnel solaire ou par la mesure précise, par télémétrie laser, du mouvement relatif de la Terre et de la Lune. De nombreuses expériences spatiales ont été proposées afin de dépasser les limitations expérimentales induites principalement par l'activité humaine, les vibrations sismiques et le gradient de gravité terrestre. La mission MICROSCOPE a été sélectionnée par le CNES avec pour objectif de tester le principe d'équivalence avec une précision améliorée de plus de deux ordres de grandeur pour atteindre 10^{-15}. Les travaux en cours ont permis de préciser les principes expérimentaux, la configuration de l'instrument et de définir la configuration du micro-satellite dédié. L'expérience consiste à tester l'universalité de la chute des corps en orbite autour de la Terre. Deux masses de forme quasi-cylindrique et de matériaux différents, alliage de Platine ou de Titane, sont finement contrôlées au moyen de forces électrostatiques afin de suivre la même orbite avec une précision meilleure que $3 \cdot 10^{-11}$ m. Les accélérations appliquées sont alors comparées avec une précision de $5 \cdot 10^{-15}$ m·s^{-2}, toute différence pointée vers la Terre est alors interprétée. En fait, le mouvement de deux masses de même matériaux est également comparé afin d'identifier les erreurs expérimentales. L'instrumentation bénéficie de nombreux développements concernant des accéléromètres électrostatiques spatiaux ultra-sensibles qui ont déjà permis la réalisation de missions spatiales pour la détermination précise du champ de gravité terrestre. Le satellite constitue un bouclier contre la traînée atmosphérique et les pressions de radiation terrestres ou solaires pour les masses d'épreuves qui ne doivent être soumises qu'au champ gravitationnel de la Terre. Pour cela, le satellite possède douze propulseurs électriques à effet hall qui sont activés continûment et dont la poussée est modulée en fonction des mesures d'accélérations appliquées aux masses. La stabilité thermique et structurale de l'instrumentation et du satellite sont optimisées ainsi que l'environnement magnétique et gravitationnel. Des efforts particuliers sont nécessaires pour éliminer les effets du gradient de gravité de la Terre ou du satellite. Le prototype de l'instrument est en cours de réalisation, le lancement du satellite étant programmé pour fin 2004. Par la démonstration de technologies spatiales innovantes, cette mission devrait ouvrir la voie à des missions futures en physique fondamentale encore plus ambitieuses et qui nécessitent comme MICROSCOPE la mesure de mouvements extrêmement faibles.

---

1. MICROSCOPE mission: context and objectives

Nowadays, experiments in gravitation deal with the two basic objectives of fundamental physics, the assessment of the general theories, general relativity in the case discussed hereafter, and the definition of all interactions in the search for grand unification. The unification of the electromagnetic and weak interaction has been carried out and the unification of these two forces with the strong force needs to be fully experimentally assessed by the direct detection of the Higgs boson, leading thus to the confirmation of the mass generation scheme of the gauge theories. Many attempts of unification of these interactions with gravity have been performed, among them string theory appears to be the most exciting.

Approaches to quantum gravity theory and to unification of all interactions lead, for most of them, to the introduction of an additional interaction depending on an additional scalar field, which couples differently to different kinds of elementary particles, and thus violates the equivalence principle.

The test of the equivalence principle is then the basic experiment among many others proposed in the domain of fundamental physics. Space programs now include many feasibility studies of experiments.

These projects concern quantum mechanics [1]: Casimir effect, quantum mechanical vacuum fluctuations, decoherence and space–time fluctuations with SQUID-based sensing instruments or atomic interferometers. They also concern special relativity: speed of light dependence and isotropy with cryogenic cavities or interferometers. Finally, they concern general relativity, weak equivalence principle for ordinary matter, charged matter or polarised matter (spin coupling), Yukawa force, gravitomagnetic and Lense–Thirring effects, determination and time constancy of the gravitational constant.

In parallel, in recent years great effort has been made by physics laboratories towards the development of various experiments dealing with the test of the equivalence principle, the research for new interactions or for new gravitational potential. The confirmation with better accuracy of the equivalence between inertial mass and gravitational mass represents an important verification of general relativity and of other metric theories of gravitation, and highlights finer determination of post-Newtonian coefficients [2]. The violation of the equivalence principle would lead to the evidence of a new interaction [3–5].

The accuracy of the determination of Newton's constant G has been recently reconsidered by an international committee because of noncoherent results depending on experimental procedures [6]. Besides, inverse square law experiments have been developed with gravimeters or gradiometers [7–9]. Galileo free fall experiments have also been performed, but with an accuracy presently limited by the effects of the Earth's gravity gradients, the fall initial conditions, the mass mutual interaction and the residual disturbances of the motions even when specific tower, gravimeter or genius double mass configuration are considered as in the Carussoto experiment, exploiting joined half discs of Be–Cu [10–12]. Beam balance configurations have also been optimised for the test of the equivalence principle [13], but the most accurate experiments exploit in-laboratory torsion pendulums. The limitations of the Cavendish configuration with attractive point masses have been over passed with the Eötvös configuration comparing the accelerations of different materials towards the Earth [14]. Solar attraction is now considered with the interest of a gravity source rotating around the torsion balance, fixed in the laboratory, and leading to the necessary modulation of the signal for the elimination of spurious disturbances [15]. After decades of optimisation of these torsion balance configurations and of their environment limiting the effects of gravity and thermal gradients, the Eöt–Wash experiment provides the best obtained results [16,17] and the necessity is now to deal with environmental instabilities induced in particular by gravity gradient fluctuations [18] and human activities. Considering the accurate measurements provided by laser ranging of the Earth–Moon relative motion in the Sun's gravity field, complementary results are deduced but interpretations are limited by the not sufficiently well identified material composition of the two celestial bodies [19].

Thus, many space experiments have also been studied and proposed in the past years to overcome the laboratory experiment limitations, but these missions have not yet been selected because they are considered by space agencies to be too complex, risky to implement and too expensive [20–23].

In this context, MICROSCOPE (MICROSatellite pour l'Observation du Principe d'Equivalence) is the first space-selected mission aiming at the EP test. The mission objective of 10^{-15} accuracy is more than two orders of magnitude better than the present ground tests. An even better accuracy has not been considered, so as to obtain an instrument compatible with the 120 kg micro-satellite, developed by Cnes and which offers many opportunities of launch as secondary passenger on ARIANE V or on Russian or Indian launchers. MICROSCOPE takes also advantage of new electrical thrusters, now available in Europe and necessary to finely and continuously control the space platform along its orbit in a quasi-pure gravitational motion. In addition, after the two flights of the ASTRE instrument on board the Columbia shuttle [24] and the recent flight of the STAR accelerometer on board the CHAMP satellite [25], electrostatic space accelerometers have now a sufficient maturity of technology to consider specific configurations with room temperature operation and ultra high sensitivities compatible with femto-g resolution [26]. Furthermore, recent altimetry and geodesy missions [27,28] lead to the global and accurate determination of the Earth's gravity field and to the production of dedicated mathematical and computational tools for accurate orbital motion simulation; this is of major interest for MICROSCOPE data processing and is analysed later in the paper.

2. Concept of the experiment

The MICROSCOPE experiment is a Galileo free fall test with two masses composed of two different materials. These masses fly in orbit around the Earth at an altitude of about 700 km and are submitted to exactly the same gravitational field. Electrostatic fields are added around the masses, breaking the experimentation symmetry, and are controlled to force them on the same orbital motion. Accurate measurements of these fields and of any defect of symmetry give rise to evidence of an EP violation (see *figure 1*).

The interest of this space experiment relies first in the expected level of residual acceleration on board the dedicated compact satellite. As an example, *figure 2* presents the variations of the accelerations measured in orbit by the STAR accelerometer on board the CHAMP Earth pointing satellite [27]. The variations are less than $4 \cdot 10^{-7}$ m·s^{-2} and further reduced levels are expected for MICROSCOPE because of higher altitude and lower atmospheric density. Moreover, a specific drag compensation system is implemented in the satellite to counteract continuously and in all directions the satellite surface forces by firing the electrical propulsion in such a way to nullify the resultant.

The second interest relies in the orbital motion allowing free fall observation periods in steady conditions over days and weeks and thus leads to the high rejection of stochastic disturbances. These periods have to be compared to the drop tower free fall duration of a few seconds and to mine experiments also limited to less than ten seconds [29].

At least, fine rotations of the instrument can be performed through the satellite attitude control thanks to the star sensors, the electrical actuators and the weak space disturbances. Then, the observational frame rotates with respect to the Earth's gravity field and the eventual EP violation signal is modulated contrarily to the instrument self-spurious disturbances and in a different way to the Earth's gravity gradient. In the MICROSCOPE experimental procedures, several rotation frequencies are considered around 10^{-3} Hz, with well-selected phases corresponding to different satellite positions along its orbit. The stability of the rate and of the rotation axis orientation is expected better than 10^{-3}, allowing fine heterodyne detection.

The satellite payload is actually composed of two near identical instruments, each including concentric and quasi-cylindrical test masses. The masses are made of the same material in the instrument 1, dedicated to determine the experiment definitive accuracy, and of different materials in the instrument 2. In view of suppressing the systematic errors, the experiment relies then, on the double comparison of the outputs of two pairs of electrostatic accelerometers, whose inertial masses are the test-masses.

The selection of the mass material is a compromise between the instrument accuracy requirements and the theoretical interest. Micrometric geometry, thermal stability and ageing, magnetic and electric properties, off gazing and chemical stability have to be considered as well as the difference of nuclei

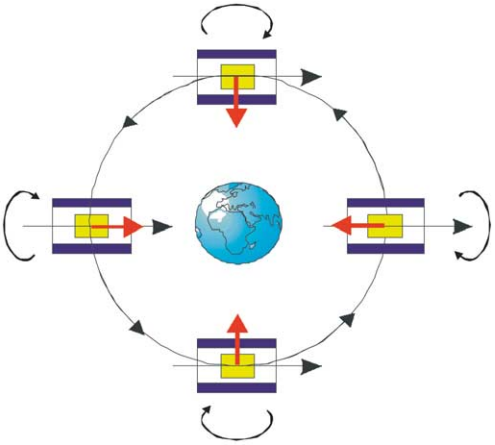

Figure 1. The MICROSCOPE experiment: shielded by the satellite, the two masses, made of different materials, fall around the Earth; they are submitted to the same gravity field and controlled along the same orbit; in case of EP violation, the electrostatic force (in red) is accurately measured towards the Earth while the instrument frame (in black) rotates.

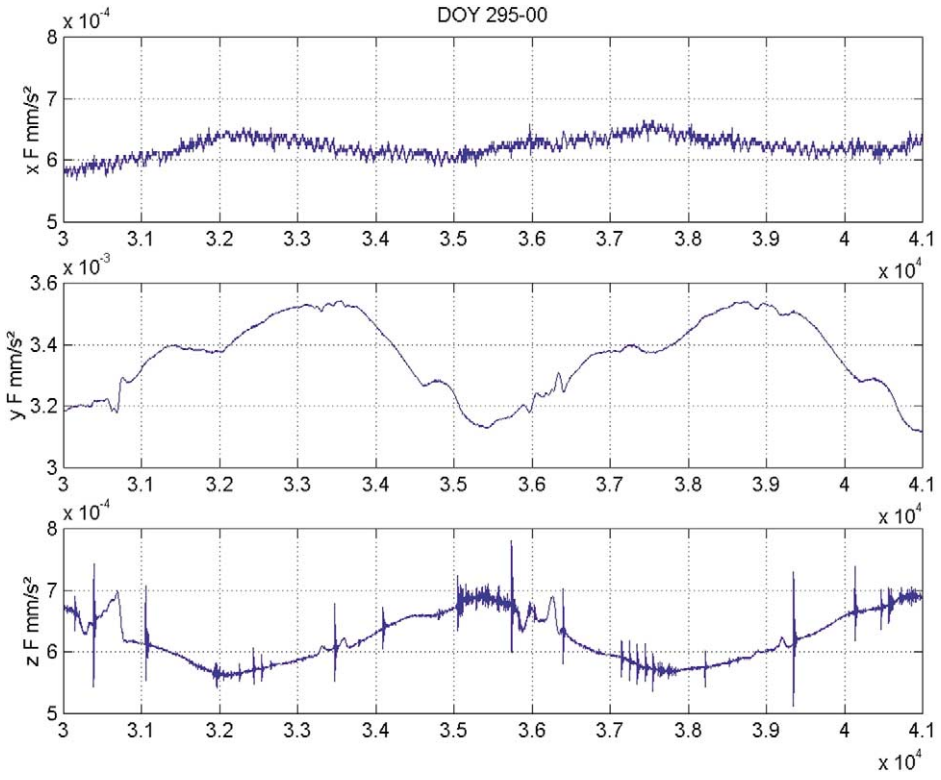

Figure 2. In-orbit accelerations measured by the STAR instrument at the centre of mass of the CHAMP satellite; along local vertical direction (upper), along satellite velocity vector (atmospheric drag) (middle) and normal to the orbit plane (lower); day 295, year 2000, about 2 orbit duration.

components related to new possible interactions [5], or to already performed EP tests [18]. Platinum and titanium alloys have been selected, with mass ranging from 0.4 kg up to 1.7 kg (see *table 1*). More couples of masses and materials are obviously of great interest but are not compatible with the integration of more instruments on board the microsatellite. The success of the mission will certainly open the door to further missions.

Table 1. Average values for typical elements and for selected platinum and titanium: proton, neutron, lepton numbers, respectively Z, N, L; new interaction, in violation to EP, could be determined by some generalised charge depending on these atomic characteristics.

Elements	Z	μ	$(N+Z)/\mu$	L/μ	$(N-Z)/\mu$
Hydrogen	1	1.00149	1.00000	0.99985	−0.99970
Beryllium	4	8.94221	1.00646	0.44732	0.11183
Carbon	6	11.91785	1.00782	0.50345	0.00093
Silicon	14	27.86754	1.00866	0.50238	0.00390
Titanium	22	47.50717	1.00891	0.46309	0.08273
Platinum	78	1193.56593	1.00801	0.40296	0.20208

3. Performance driving parameters

The motion of the masses is finely measured with respect to the highly stable silica frame of the instrument by sets of capacitive position sensors. According to the electronic circuit performance and to the electrode geometry, accuracy of $3 \cdot 10^{-11}$ m·Hz$^{-1/2}$ is expected and the relative position of the two masses is maintained motionless by electrostatic forces. The fine comparison of these control forces performed with an accuracy of $5 \cdot 10^{-13}$ N·Hz$^{-1/2}$ leads to the EP test with the expected 10^{-15} accuracy, considering an integrating period of about one day. The motion of each mass can be simply expressed by:

$$m_{\mathrm{IA}}(\ddot{X}_{\mathrm{A}} + \ddot{x}_{\mathrm{A}}) - m_{\mathrm{gA}} g_{\mathrm{A}} = F_{\mathrm{A}} + F_{\mathrm{pA}}$$

with the index A (or B later) to identify the mass, the index I or g for inertial or gravitational mass, X the displacement of the instrument structure (linked to the satellite) with respect to the inertial frame and x of the mass with respect to the instrument, g_{A} the Earth gravitational field integrated over the mass volume, F_{A} and F_{pA} the electrostatic applied force and other disturbing force.

Then, the difference of the two measured electrostatic forces becomes:

$$\begin{aligned}
\frac{\widehat{F}_{\mathrm{A}}}{m_{\mathrm{IA}}} - \frac{\widehat{F}_{\mathrm{B}}}{m_{\mathrm{IB}}} \approx & +(K_{\mathrm{A}} - K_{\mathrm{B}}) \frac{\ddot{X}_{\mathrm{A}} + \ddot{x}_{\mathrm{A}} - g_{\mathrm{A}} + \ddot{X}_{\mathrm{B}} + \ddot{x}_{\mathrm{B}} - g_{\mathrm{B}}}{2} + \left(I + \frac{(K_{\mathrm{A}} + K_{\mathrm{B}})}{2} \right) (\ddot{X}_{\mathrm{A}} - \ddot{X}_{\mathrm{B}}) \\
& + \left(I + \frac{(K_{\mathrm{A}} + K_{\mathrm{B}})}{2} \right) \left\{ (\ddot{x}_{\mathrm{A}} - \ddot{x}_{\mathrm{B}}) + 2\Omega(\ddot{x}_{\mathrm{A}} - \ddot{x}_{\mathrm{B}}) + (\Omega \times \Omega + \dot{\Omega})(x_{\mathrm{A}} - x_{\mathrm{B}}) \right\} \\
& - \frac{1}{2} \left(\frac{m_{\mathrm{gA}}}{m_{\mathrm{IA}}} + \frac{m_{\mathrm{gB}}}{m_{\mathrm{IB}}} \right) (g_{\mathrm{A}} - g_{\mathrm{B}}) - \left(\frac{m_{\mathrm{gA}}}{m_{\mathrm{IA}}} - \frac{m_{\mathrm{gB}}}{m_{\mathrm{IB}}} \right) \left(\frac{g_{\mathrm{A}} + g_{\mathrm{B}}}{2} \right) - \frac{\widehat{F}_{\mathrm{pA}}}{m_{\mathrm{IA}}} + \frac{\widehat{F}_{\mathrm{pB}}}{m_{\mathrm{IB}}} \\
& + E(F_{\mathrm{A}}) - E(F_{\mathrm{B}}) + E_{\mathrm{nA}} - E_{\mathrm{nB}}
\end{aligned} \tag{1}$$

where $\widehat{F}_{\mathrm{A}}/m_{\mathrm{IA}}$ is the measurement of the electrostatic applied acceleration depending on the sensitivity matrix K_{A}, the non-linearity $E(F_{\mathrm{A}})$ and the pick-up electronics noise E_{nA}.

The first term corresponds to the mass common mode acceleration that is not fully suppressed because of the difference of instrument sensitivities; second and third to the relative residual motion of the masses, with Ω the angular velocity of the instrument about the in-orbit freefall point. The derivatives in the third term are performed in the rotating frame. The fourth reflects spatial variations of the gravity that can be expressed, as later, with $[\boldsymbol{T}]$ the gradient tensor. The fifth corresponds to the EP test signal, the two last terms expressing the instrument errors.

The atmospheric and thermal drag of the satellite are actively controlled in such a way that the satellite follows the two test masses in their gravitational motion leading to nullify $\frac{1}{2}(\ddot{X}_{\mathrm{A}} + \ddot{x}_{\mathrm{A}} - g_{\mathrm{A}} + \ddot{X}_{\mathrm{B}} + \ddot{x}_{\mathrm{B}} - g_{\mathrm{B}})$. The satellite attitude control system also limits the erratic evolutions of Ω, leading to inertial acceleration of a few 10^{-10} m·s^{-2} because the mass distances are less than 20 µm by construction, the gravity gradient contribution being then of a few 10^{-11} m·s^{-2}. The eventual equivalence principle (EP) signal of a few 10^{-15} m·s^{-2} has thus to be detected through the very different temporal spectra.

To show the logic of the proposed data processing, let us only consider the monopolar term of the Earth's gravity in an Earth fixed frame; the quadripolar contribution, three orders of magnitude smaller, and the other spherical harmonics are neglected here:

$$g_i = -\frac{\mu}{r^2} \frac{x_i}{r}, \quad \text{and} \tag{2}$$

$$T_{ij} = -\frac{\mu}{r^3} \left[\delta_{ij} - 3 \frac{x_i}{r} \frac{x_j}{r} \right] \tag{3}$$

with $\mu \approx 4 \cdot 10^{-14}$ m^3·kg^{-1}·s^{-2}, the Earth gravitational constant and r the distance to the geocentre, $r = (x_1^2 + x_2^2 + x_3^2)^{1/2}$ (x_i the rectangular co-ordinates of the current point in Earth's fixed orthonormal frame); δ_{ij} is the Kronecker symbol.

With this monopole approximation, these expressions remain identical in other frames deduced by rotation from the Earth fixed frame, as the orthonormal nodal frame $[h, k, w]$: h along the ascending node of the orbit, w along the angular momentum of the satellite (normal to the orbital plane). This frame is quasi-inertial (it undergoes only the slow rotation of the node) and allows highlighting of the temporal variations of the satellite coordinates:

$$\begin{aligned}
\frac{x_1}{r} &= \cos(f+\omega) = \cos\lambda + e\cos(2\lambda-\omega) - e\cos\omega + \mathrm{O}\big(e^2\big)\\
\frac{x_2}{r} &= \sin(f+\omega) = \sin\lambda + e\sin(2\lambda-\omega) - e\sin\omega + \mathrm{O}\big(e^2\big)\\
\frac{x_3}{r} &= 0\\
\frac{r}{a} &= 1 - e\cos f + \mathrm{O}\big(e^2\big) = 1 - e\cos(\lambda-\omega) + \mathrm{O}\big(e^2\big)
\end{aligned} \tag{4}$$

where f is the true anomaly of the satellite orbit, a, e and ω respectively the semi-major axis, the eccentricity and the argument of the perigee, and $\lambda = M + \omega$ (M mean anomaly) is the mean argument of the latitude. λ is a fast angle which has a frequency $f_{\mathrm{EP}} \approx n = 1/2\pi(\mu/a^3)^{1/2}$ whereas ω has a low frequency (about 10^3 smaller than f_{EP}).

Substituting equation (4) into (2) and (3), the following expressions of the gravity vector and gradient tensor are obtained in the nodal frame:

$$\begin{aligned}
g_1 &= -\frac{\mu}{a^2}\big[\cos\lambda + 2e\cos(2\lambda-\omega)\big] + \mathrm{O}\big(e^2\big)\\
g_2 &= -\frac{\mu}{a^2}\big[\sin\lambda + 2e\sin(2\lambda-\omega)\big] + \mathrm{O}\big(e^2\big)\\
g_3 &= 0
\end{aligned} \tag{5}$$

$$\begin{aligned}
T_{11} &= \frac{1}{2}\frac{\mu}{a^3}\left[1 + 3\cos(2\lambda) + e\left(-\frac{3}{2}\cos(\lambda+\omega) + 3\cos(\lambda-\omega) + \frac{21}{2}\cos(3\lambda-\omega)\right)\right] + \mathrm{O}\big(e^2\big)\\
T_{12} &= \frac{1}{2}\frac{\mu}{a^3}\left[3\sin(2\lambda) + e\left(-\frac{3}{2}\sin(\lambda+\omega) + \frac{21}{2}\sin(3\lambda-\omega)\right)\right] + \mathrm{O}\big(e^2\big)\\
T_{13} &= 0\\
T_{22} &= \frac{1}{2}\frac{\mu}{a^3}\left[1 - 3\cos(2\lambda) + e\left(\frac{3}{2}\cos(\lambda+\omega) + 3\cos(\lambda-\omega) - \frac{21}{2}\cos(3\lambda-\omega)\right)\right] + \mathrm{O}\big(e^2\big)\\
T_{23} &= 0\\
T_{33} &= -\frac{\mu}{a^3}\big[1 + 3e\cos(\lambda-\omega)\big] + \mathrm{O}\big(e^2\big)
\end{aligned} \tag{6}$$

If the satellite is not spinning (i.e. quasi-inertial pointing), these are also the components in the instrumental frame up to a constant phase. It clearly appears that the main contribution of the EP signal is in the orbital plane at the frequency f_{EP} (spectral line 1 for short) while the components of the gravity gradient in the orbital plane have essentially the frequency 2 f_{EP} (spectral line 2). However, it is important to notice the $\mathrm{O}(e)$ contribution of the gravity gradient to the spectral line 1. This shows that it is necessary to compute some off centring thanks to the large signal at spectral line 2 in order to discriminate the EP contribution in line 1. This is the selected strategy, considering that the accelerometer measurements are irrelevant at very low frequencies and in particular at DC. Centring accuracy of 0.1 µm is expected with two envisaged approaches: to correct a posteriori the measurement data or to centre in flight the test masses by biasing the position capacitive sensors in the accelerometer servo-loops (***figure 5***).

The situation is slightly different when the satellite rotates around the normal to the orbital plane; setting the slowly varying angle ω to 0 (in order to simplify the presented analysis), we have in this case:

$$
\begin{aligned}
g_1 &= -\frac{\mu}{a^2}\left[\cos(a_{\mathrm{EP}}) + 2e\cos(a_{\mathrm{EP}}+\lambda)\right] + \mathrm{O}\left(e^2\right)\\
g_2 &= -\frac{\mu}{a^2}\left[\sin(a_{\mathrm{EP}}) + 2e\sin(a_{\mathrm{EP}}+\lambda)\right] + \mathrm{O}\left(e^2\right)\\
g_3 &= 0
\end{aligned}
\tag{7}
$$

$$
\begin{aligned}
T_{11} &= \frac{1}{2}\frac{\mu}{a^3}\left[1 + 3\cos(2a_{\mathrm{EP}}) + e\left(-\frac{3}{2}\cos(2a_{\mathrm{EP}}-\lambda) + \frac{21}{2}\cos(2a_{\mathrm{EP}}+\lambda) + 3e\cos\lambda\right)\right] + \mathrm{O}\left(e^2\right)\\
T_{12} &= \frac{1}{2}\frac{\mu}{a^3}\left[3\sin(2a_{\mathrm{EP}}) + e\left(-\frac{3}{2}\sin(2a_{\mathrm{EP}}-\lambda) + \frac{21}{2}\sin(2a_{\mathrm{EP}}+\lambda)\right)\right] + \mathrm{O}\left(e^2\right)\\
T_{13} &= 0\\
T_{22} &= \frac{1}{2}\frac{\mu}{a^3}\left[1 - 3\cos(2a_{\mathrm{EP}}) + e\left(\frac{3}{2}\cos(2a_{\mathrm{EP}}-\lambda) - \frac{21}{2}\cos(2a_{\mathrm{EP}}+\lambda) + 3\cos\lambda\right)\right] + \mathrm{O}\left(e^2\right)\\
T_{23} &= 0\\
T_{33} &= -\frac{\mu}{a^3}[1 + 3e\cos\lambda] + \mathrm{O}\left(e^2\right)
\end{aligned}
\tag{8}
$$

where $a_{\mathrm{EP}} = \lambda - s$ (s counted positively in the same sense as the mean anomaly) is the argument of the EP main signal. The great advantage of this rotation is that the gravity gradient has no longer a significant contribution at the EP frequency.

The tensor of inertia has essentially constant components in the instrumental frame and will not be further analysed here.

From (5), the semi-major axis has to be minimised to maximise the EP signal proportional to g. However, the altitude must be sufficiently high to reduce the atmospheric drag. Hence, the most interesting value for the altitude is about 700 km ($g \approx 8.2$ m·s^{-2}) where the forces due to the drag and the solar radiation pressure are nearly equal, but 1500 km ($g \approx 6.4$ m·s^{-2}) is still acceptable. Equations (5) and (7) also show that the sensitive axis of the instrument must lie in the orbital plane.

The eccentricity must be small for two reasons: (i) to concentrate the power spectrum of the EP signal in a unique line (spectral line 1), and (ii) to limit the contribution of the gravity gradient at spectral line 1 when the satellite is not spun. In the MICROSCOPE mission we will be able to recover the in-plane off centring with an accuracy better than 10^{-7} m. That is why the eccentricity must be smaller than $5 \cdot 10^{-3}$, to limit the perturbations due to the gravity gradient in the case of null spin.

The knowledge of the position of the satellite is necessary to compute the gravity gradient. Given the components Δx_j of the mass off centring and the errors ΔX_k on the satellite position, the induced error on the estimated differential acceleration due to the gravity gradient is:

$$
\Delta\Gamma_i = \sum_{j=1}^{3}\sum_{k=1}^{3}\frac{\partial^2 g_i}{\partial x_j \partial x_k}\Delta x_j \Delta X_k \tag{9}
$$

When expressed in the instrumental frame, these derivatives with magnitudes of the order of μ/a^4 (a few 10^{-13} m^{-1}·s^{-2} for an altitude of 700 km) have their main contribution, i.e. terms independent on the eccentricity, at the EP frequency. Spinning the instrument does not reject all these terms at other frequencies. Considering the nominal mass off centring of $2 \cdot 10^{-5}$ m, the uncertainty ΔX_i of the satellite position must not exceed 300 m at frequencies 0, f_{EP} and 2 f_{EP} in the instrumental frame.

Moreover, in case of a small inclination ε of the instrument from the orbital plane, it becomes sensitive to the out of plane component of the off centring: T_{13} and T_{23} have contributions $\mathrm{O}(e\sin\varepsilon)$ which are at the EP frequency in the case of null spin; this leads to induced acceleration $(\mu/r^3)e\sin(\varepsilon)\Delta x_3 \approx 2 \cdot 10^{-13}\varepsilon$ for

$\Delta x_3 = 2 \cdot 10^{-5}$ m. Thus, the instrument sensitive axis must be controlled in the orbital plane with a better accuracy than $5 \cdot 10^{-3}$ rad. This requirement, which depends on the eccentricity of the orbit, can be relaxed in spun mode. A more detailed analysis, taking into account the geometric characteristics of the instrument and their stability, evidences other constrains on the stability of the angular velocity and acceleration of the rotating satellite. In addition, the knowledge of the instrument orientation with $5 \cdot 10^{-3}$ rad accuracy is also necessary to compute the gravity gradient and to obtain 0.5% relative accuracy of the mass off centring.

While the measurement relies on a specific filtering data process over one to two days, longer durations can be used to improve the signal to noise ratio in the recovery of the EP eventual violation signal. But most of the mission duration is devoted to the validity of the experiment data process and to the verification of the instrument accuracy and sensitivity. Mainly, three types of parameters appear essential in the signal composition shown in the previous equation (1): the sensitivity matrix of the differential accelerometers, the parasitic forces and the test-mass centring, already considered.

The sensitivity matrix represents the instrument scale factors, the test-mass alignments and the couplings. Well-defined cinematic accelerations of the satellite can be induced with the field emission electric propulsion (FEEP) system of the satellite [30,31]. By comparing the outputs of the accelerometers along all directions and whether the accelerometer participates or not to the satellite motion control, matching of the characteristics can be performed with the expected relative accuracy of 10^{-4}.

The thermal sensitivity and the magnetic sensitivity of the instrument can be handled with smart location of thermoresistors and current loops. This is to be implemented in the satellite according to interface and integration possibilities.

4. MICROSCOPE instrument

The MICROSCOPE payload has been designed from the concept and the technology optimised with the ultra-sensitive space accelerometers based on the electrostatic levitation of a solid mass in a highly accurate and stable instrument cage. These tri-axial accelerometers, which have been designed and qualified for the CHAMP [27] and GRACE [28] missions are now being developed for the GOCE mission [32].

Each of the two instruments is composed of two concentric electrostatic accelerometers with quasi-cylindrical test masses exhibiting a spherical matrix of inertia to reduce the effects of local gravity gradient fluctuations; sizes have been selected to limit furthermore the effects of different high order gravitational multipoles. All around the mass, pairs of electrodes are engraved in the accelerometer core, made of gold-coated fused silica for the capacitive sensing of the mass position and attitude (see *figure 3*).

The eight quadrant electrodes concern the radial translations and rotations, the two cylindrical sensing electrodes at the ends of the test-mass are used for the axial direction. The rotation of the mass about the axial direction is measured through dedicated flat areas on the mass and external specific electrodes.

This configuration has been optimised to reduce the electrostatic stiffness and damping applied to the mass and associated in particular to the sensing of electrical signals. The same electrodes are used to generate electrostatic fields for the servo-control of the mass, which is maintained motionless with respect

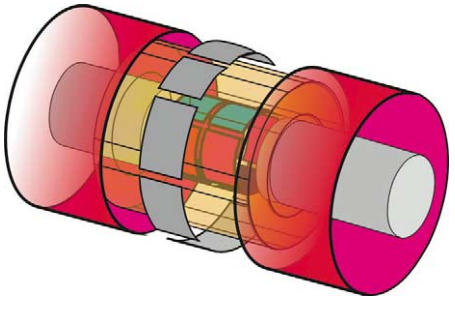

Figure 3. Electrode configuration around the test-mass (yellow).

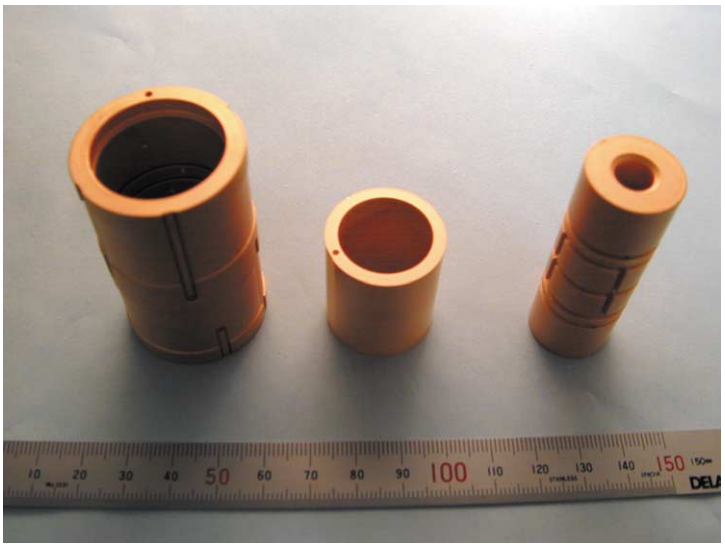

Figure 4. First prototype: the gold coated silica mass between the outer cylinder (left) and the inner cylinder (right).

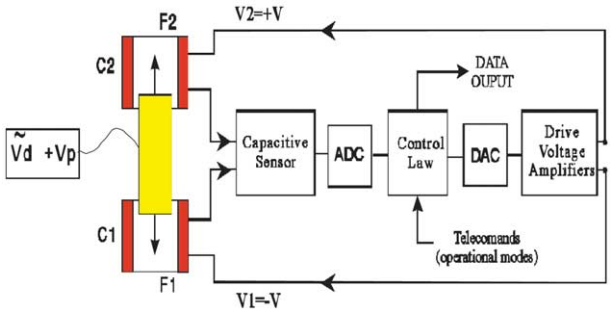

Figure 5. Electrostatic loop configuration: the capacitances C1 and C2 are maintained equal by applying the voltages V1 and V2 to maintain the mass motionless at the centre. Six loops similar to this one are considered by mass.

to the silica instrument frame. The resultant of the generated electrostatic forces is derived from the accurate measurement of the applied voltages on the pairs of electrodes (see *figure 5*).

The mean force applied on both masses of the same instrument is in fact maintained null thanks to the satellite drag compensation system that acts on the thrusters to move the satellite and hence the instrument silica frame following the masses. The difference of the electrostatic forces is then observed along the orbit to search of any EP violating signal. The relative position of the masses can be modified by offsetting the electrostatic servo-loops: verification of the instrument sensitivity to this parameter will be performed during the calibration phase as well as the rejection rate of the Earth gravity gradient signal.

Both instrument cores are integrated in tight vacuum housings that also provide thermal inertia and insulation, plus magnetic shielding (see *figure 6*): fluctuations of the instrument temperature are controlled at setting plane by the satellite sub-system. These housings are mounted near the satellite centre of mass but no stringent requirement is considered because of the satellite drag-free control.

The total mass of the payload is estimated to be 40 kg including the two instrument cores and the electronics units which include the mass servo-loop controls, the data and power interfaces and the instrument operation controller, and which consume an overall power of less than 40 Watts.

The resolution of the instrument is evaluated from the electronics' noise levels, as measured in the laboratory, from the mass motion perturbing sources, as modelled after experimental investigations and from the instrument environment sensitivity. The performances are optimised at frequencies around 10^{-3} Hz, corresponding to $f_{\rm EP}$ in the case of a rotating satellite.

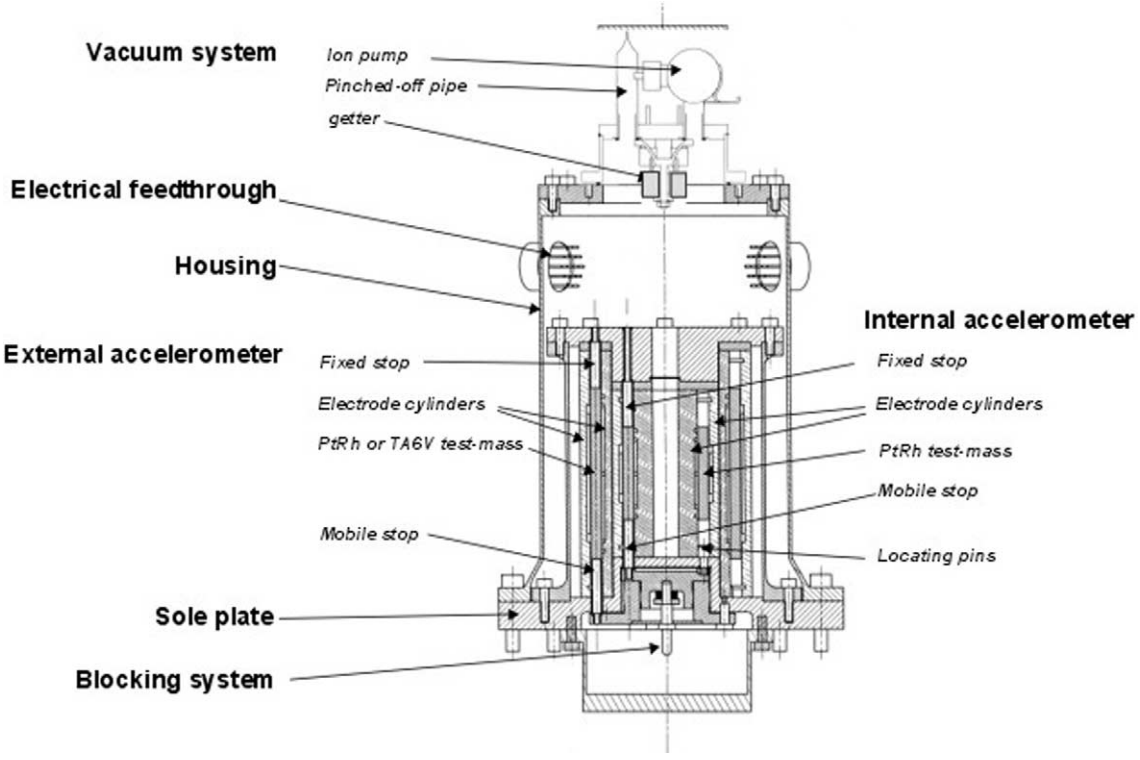

Figure 6. Configuration of one instrument's mechanical core, composed of two concentric electrostatic accelerometers (the electronics unit is not shown).

At frequencies lower than 10^{-3} Hz, the thermal instabilities ΔT at the instrument interface induce radiation pressure and radiometer acceleration fluctuations due, for the later, to the residual gas pressure P inside the tight housing, i.e. in PSD:

$$\Gamma^2_{\text{radiometer}} \approx \left(\frac{1}{2m} PS \frac{\Delta T}{T\sqrt{1+(2\pi\tau_{\text{e}} f_{\text{EP}})^2}} \right)^2 \left(\text{m}\cdot\text{s}^{-2}\right)^2 \cdot \text{Hz}^{-1}$$

with m the mass of the test-mass, S its area normal to the thermal gradient direction, and τ_{e} the thermal time constant (considered greater than 3 hours) from interface to the core facing the test-mass. A residual pressure of 10^{-5} Pa has already been obtained with such a technology and is sufficient to limit the radiometer effect to much less than the required value of $5 \cdot 10^{-13}$ m·s^{-2}·Hz$^{-1/2}$ when considering the temperature fluctuations of *table 2*.

Table 2. Thermal characteristics required by both payload units (PSD: Power Spectrum Density).

	Electronics unit	Mechanics unit
Operating temperature	$+10$ °C/$+50$ °C	$+20$ °C/$+40$ °C
Thermal variations PSD (about f_{EP})	1 K·Hz$^{-1/2}$	0.1 K·Hz$^{-1/2}$
Thermal variations Tone (sine at f_{EP})	3 mK	0.3 mK
Thermal gradients PSD (about f_{EP})	No	1 K·m^{-1}·Hz$^{-1/2}$
Thermal gradients Tone (sine at f_{EP})	No	0.003 K·m^{-1}

Table 3. Instrument range of operation in the two operating modes; performance for the EP test are obtained in measurement mode; resolution is 100 less in safe mode but the electrostatic levitation of the mass can be acquired while the drag-free system is not operating.

Accelerometer axes	Safe mode	Measurement mode
X (axial)	5×10^{-6} m·s^{-2}	10^{-7} m·s^{-2}
Y and Z (radial)	5×10^{-5} m·s^{-2}	5×10^{-6} m·s^{-2}
Rotation about X	10^{-5} rad·s^{-2}	10^{-6} rad·s^{-2}
Rotation about Y or Z	10^{-4} rad·s^{-2}	10^{-5} rad·s^{-2}

At frequencies higher than 10^{-2} Hz, the position sensing resolution x_{noise} affects the resolution with a square frequency law, i.e. in PSD:

$$\Gamma^2_{\mathrm{posnoise}} = x^2_{\mathrm{noise}}\left(4\pi^2 f^2_{\mathrm{EP}} + 4\pi^2 f^2_{\mathrm{p}}\right)^2 \left(\mathrm{m{\cdot}s^{-2}}\right)^2 \cdot \mathrm{Hz}^{-1}$$

with f_{p} the frequency associated to the residual passive stiffness between the mass and the instrument structure (different from the active servo-loop one), which is evaluated to be less than $5 \cdot 10^{-6}$ N·m^{-1}, and so 'negligible' effects have to be considered at lower frequencies.

About f_{EP} frequency, the thermal noise of the mass motion is the major source of error, greater than the back action of the electronics, the pick-up measurement noise, and magnetic or electric effects due to mass residual susceptibility or contact potential differences. Derived from dissipation–fluctuation theorem, the expression depends on the damping factor (which does not include the electrostatic cold damping of the servo-loops) estimated from dedicated laboratory experiments and mainly due to the thin 5 µm wire used for the charge control of the mass, i.e. in PSD:

$$\Gamma^2_{\mathrm{wire}} = \left(\frac{1}{m}\sqrt{4k_{\mathrm{B}}T\frac{k_{\mathrm{wire}}}{2\pi f_{\mathrm{EP}} Q_{\mathrm{wire}}}}\right)^2 \left(\mathrm{m{\cdot}s^{-2}}\right)^2 \cdot \mathrm{Hz}^{-1}$$

k_{wire} and Q_{wire} are respectively evaluated to $5 \cdot 10^{-6}$ N·m^{-1} and 100 at 10^{-3} Hz [33,34]. The quadratic sum of all considered noise sources leads then for each mass to a maximum of $1.5 \cdot 10^{-12}$ m·s^{-2}·Hz$^{-1/2}$.

Besides the instrument resolution, the thermal stability of the accelerometer sensitivity and bias has been considered as well as the linearity. Thanks to the satellite thermal environment stability and to the drag-free system, which limits the range of residual accelerations, these requirements appear less stringent. Robustness of the instrument operation is also considered and two ranges of operation have been defined as shown in *table 3*.

5. MICROSCOPE satellite

The MICROSCOPE mission has been implemented in the CNES (French space agency) program of 2000, within the framework of the Microsatellite Line of Product called MYRIADE. The main objective of MYRIADE is to offer the possibility of space scientific missions with low cost, reduced development time and compatible with Ariane V ASAP launch. The MYRIADE program started with the DEMETER satellite (Detection of Electro-Magnetic Emissions Transmitted from Earthquake Region) to be launched by the end of 2002. DEMETER is actually the basis of design for the follow-on missions.

Due to MICROSCOPE specifications, this baseline is updated to include fine motion and attitude control of the satellite and a peculiar steady thermal behaviour of the payload. The Sun synchronous circular orbit is selected at 670 km altitude and with 18 h 00 local time at the ascending node. It enables the keeping of the satellite in a steady orientation with respect to the Sun and then optimises the solar panel power conversion,

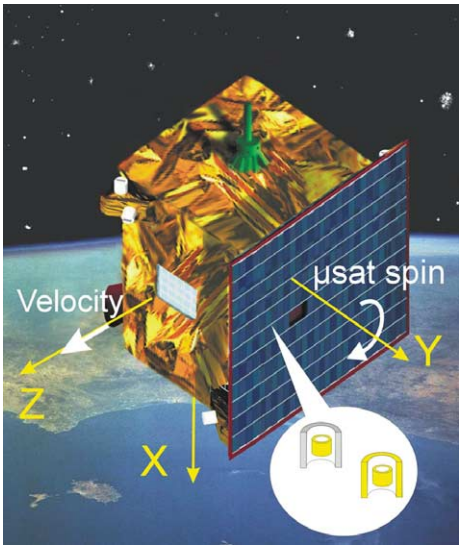

Figure 7. General configuration of the satellite.

the thermal environment stability on board and the thermo-elastic behaviour of the satellite structure. The payload thermal environment is specified in *table 2*.

The general configuration of the satellite, presented in *figure 7*, exhibits a rough cubic volume of 60 cm square by 80 cm, a 120 kg weight and a rigid and compact structure with no deployable solar panel. Any mass motion on-board is avoided and no momentum wheel is used during the operation of the experiment.

The thermo-elastic behaviour of the satellite is carefully optimised to avoid contraction fluctuations and vibrations. The structure is realised with aluminium honeycomb and plates. One solar panel is mounted on the side facing the Sun with high-efficiency AsGa solar cells. The available power of 80 W will be shared by the payload, the satellite module and the electrical propulsion system.

The magnetic cleanliness of the satellite has been ensured to reduce on one hand the satellite residual moment to less than 1 $A{\cdot}m^2$ in order to limit the torque induced by the crossed Earth magnetic field and on the other hand any residual moment variations because of the test mass non-null susceptibility: magneto-torquers, batteries, electronics wiring and solar panels are specifically concerned.

During the mission, the satellite is quasi-inertial pointing or rotating about the Y-axis, normal to the orbital plane, with low angular rates near $4 \cdot 10^{-3}$ $rad{\cdot}s^{-1}$. The residual acceleration of the satellite and its attitude are continuously controlled by acting electrical proportional thrusters, FEEP (field effect electrical propulsion). The servo of the six degrees of freedom is performed from the payload linear acceleration outputs and from the hybridisation of the star sensor and the payload angular acceleration measurements. Performance of the control is mainly limited by the fluctuations of the amplitude and the direction of the thrust provided by the sets of FEEP. Thus, each FEEP thruster must present a maximum thrust of 50 to 100 μN with a quantification step of 0.1 μN. Four pods of three electrical thrusters are located at the corners of two opposite faces of the satellite. A minimum of eight thrusters enables the full control of the satellite but twelve thrusters allows one failure redundancy and the reduction of the maximum needed thrust range. FEEP technology will be tested in orbit for the first time with the MICROSCOPE satellite. Ground performance tests have already been performed in our laboratory with indium thrusters developed by Austrian research centre Seibersdorf [35], as shown in *figure 8*.

The performance, provided in *table 4*, and presently assessed by the computerised simulation of the satellite control are compatible with the experiment accuracy.

The MICROSCOPE mission duration is one year. After the orbit injection, the satellite is controlled in safe mode, Earth pointing, with the nominal equipment of the micro-satellite platform: sun sensor and star

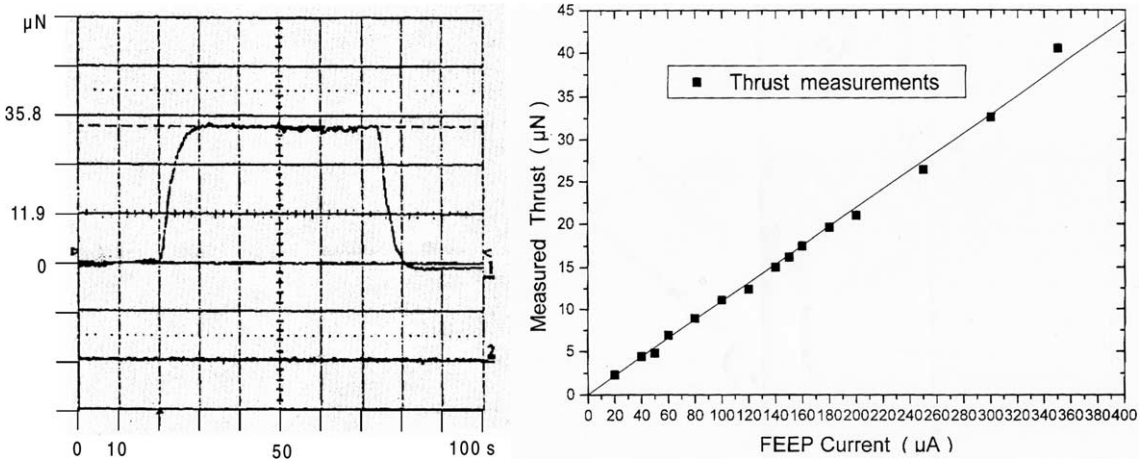

(a) (b)

Figure 8. FEEP thrust measurements performed with a dedicated balance in the ONERA vacuum chamber facility: 33 μN step of thrust (left); thrust versus ion emitter current (right).

Table 4. Attitude control of the satellite and the compensation of the drag: expected levels and noise compatible with MICROSCOPE EP experiment accuracy.

	Max. value at DC	Stability at $f_{\rm EP}$
Angular velocity	10^{-5} rad·s^{-1} or $4 \cdot 10^{-3}$ rad·s^{-1} (rotation)	10^{-6} rad·s^{-1}·Hz$^{-1/2}$
Angular acceleration	$3 \cdot 10^{-7}$ rad·s^{-2} (10^{-5} rad·s^{-2} about Y)	$3 \cdot 10^{-8}$ rad·s^{-2}·Hz$^{-1/2}$
Linear acceleration	10^{-9} m·s^{-2}	$3 \cdot 10^{-10}$ m·s^{-2}·Hz$^{-1/2}$

tracker, magneto-torquers and reaction wheels. Then, the two instruments are switched on, one by one, their operations are verified and the satellite electrical propulsion is calibrated. The satellite mass centring and its structural behaviour are verified before the drag-free and the fine-attitude control is switched on. Then the highest sensibility of the accelerometer is selected; the instruments and the satellite control are accurately characterised: residual acceleration levels, stability of rotation axis and frequency, coupling between axes, instrument sensitivity to environment and gravity gradients. After all calibrations, the EP experiment is realised with the first instrument in inertial and rotating attitudes, and with two angular phases along the orbit (defined at the equator passage). The drag-free system nullifies the common measured accelerations of this instrument, the second instrument is used to control the attitude and to survey all applied levels. In order to verify that no severe drifts have occurred between the beginning and the end of the experiment, the previous phase of calibration is performed again. The EP experiment is then performed with the second instrument with a new calibration at the end. According to the required integration periods for the filtering of the data, the minimum duration of the overall procedure is evaluated to 6 months. The extra time will be used to assess the experiment and to perform complementary operations. The total data flow rate is evaluated to be 5.5 kbit·s^{-1}, so about 480 Mbits per day. The satellite memory of 1 Gbit capacity and the rate of the TM/TC link to the ground station of 400 kbit·s^{-1} are compatible with the payload needs.

6. Conclusion

Beside the definition of the space experiment aiming at the test of the EP with an accuracy of 10^{-15}, the design of the satellite and the in orbit configuration of the payload, the first prototype of the MICROSCOPE

instrument has been defined with a configuration compatible with the operation under normal gravity in order to verify the selected configuration and the operation software. This instrument is under integration and will be tested with light masses made of silica and aluminium that can be levitated in the laboratory. Free fall testing is also scheduled in the following months at the specific drop tower of the University of Bremen: 4 seconds of nanogravity observation are expected requiring a falling double capsule, now under development to much reduce the drag due to the residual pressure inside the tower tube. The resolution of the two electrostatic accelerometers constituting the instrument cannot be fully demonstrated up to the mission required values with these tests because of the too-noisy environment and the limited time of observation: a factor of ten to one hundred shall have to be extrapolated. Fortunately, the present design of the digital servo-loop electronics permit the in orbit calibration of the instrument and the setting of the operation parameters [34].

Two other space missions, even more ambitious in term of detection of weak acceleration, are presently studied and will benefit from the MICROSCOPE acquired experience.

The LISA space mission (Laser Interferometer Space Antenna) aims at the observation of the low-frequency astrophysical gravitational radiation with cosmological and fundamental physics objectives (see Rüdiger et al. in this issue). The laser interferometer is realised with a triangle formation of three drag-free spacecraft in heliocentric orbit. At the centre of the satellite, the proof-masses of inertial sensors are the mirrors at each end of the $5 \cdot 10^6$ km interferometer arms. Then, they constitute the inertial references, free of any acceleration disturbances, with an expected level of a few 10^{-15} m·s^{-2}·Hz$^{-1/2}$ in the very low frequency domain from 10^{-4} Hz up to 10^{-2} Hz [36]. Furthermore, the inertial sensors are used by the drag-free satellite sub-system similar to the MICROSCOPE one. So, the satellite carries the highly stable interferometer optical bench and constitutes a shield for the mass that the satellite follows accurately.

The STEP mission envisages increasing the EP test accuracy by three orders of magnitude better than MICROSCOPE, taking advantage of cryogenic temperature. Masses are maintained by superconductive magnetic loops and electrostatic positioners in the instrument silica cage inside the 500 l He Dewar. SQUID sensors are used to measure the variations of the mass distances along the Earth direction.

By the demonstration of the involved space technologies and the weak acceleration measurement at femto-gravity level, MICROSCOPE opens the way to a new range of fundamental physics experiments in space, which should be performed in the first quarter of this new century to complete our knowledge of gravity.

Acknowledgements. The authors would like to acknowledge MICROSCOPE team members at Onera, Observatoire de la Côte d'Azur, Cnes and the University of Bremen.

References

[1] Respectively space proposed missions: CASIMIR, HYPER, OPTIS, MOSS, GPC, ASTROD, SPACETIME, see F2/F3 ESA proposals, February 2000.
[2] Nordtvedt K., Astrophys. J. 407 (1993) 758.
[3] Isham C.J., Class. Quantum Grav. 13 (1996).
[4] Haugan M.P., Lammerzahl C., Principles of equivalence: their role in gravitation physics and experiments that test them, in: Gyros, Clocks, Interferometers…: Testing Relativistic Gravity in Space, Lecture Notes in Physics, Springer, 2000.
[5] Damour T., Polyakov A.M., Nucl. Phys. B 423 (1994) 532.
[6] Mohr P.J., Taylor B.N., Codata recommended values of the fundamental physical constants: 1998, J. Phys. Chem. Ref. Data 28 (6) (1999);
Mohr P.J., Taylor B.N., Rev. Mod. Phys. 178 (2) (2000).
[7] Yu H.T. et al., Experimental determination of the gravitational forces at separations around 10 meters, Phys. Rev. D 2 (1979) 1813–1815.
[8] Speake C.C. et al., Test of the inverse-square law of gravitation using the 300 m tower of Erie, Colorado, Phys. Rev. Lett. 65 (1990) 1967–1971.
[9] Moody M.V., Paik H.J., Gauss's law test of gravity at short range, Phys. Rev. Lett. 70 (1993) 1195–1198.

[10] K. Kuroda, Mio N., Test of a composition dependant force by a free fall interferometer, Phys. Rev. Lett. 62 (1989) 1941–1944.
[11] Dittus H., Drop tower 'Bremen': a weightlessness laboratory on Earth, Endaveour, New Series 15 (2) (1991).
[12] Carussoto S. et al., Test of g universality with a Galileo type experiment, Phys. Rev. Lett. 69 (1992) 1722–1725.
[13] Speake C.C., Quinn T., Search for a short-range isospin-coupling component of the fifth force with use of a beam balance, Phys. Rev. Lett. 61 (1988) 1340–1343.
[14] Eötvös R.V., Pekar D., Fekete E., Beiträge zum gesetze der proportionalität von trägheit und gravität, Ann. Phys. 68 (1922) 11–66.
[15] Roll P.G., Krotlov R., Dicke R.H., The equivalence of inertial and passive gravitational mass, Ann. Phys. (USA) 26 (1964) 442–517.
[16] Adelberger E.G. et al., Phys. Rev. D 42 (1990) 3267.
[17] Su Y. et al., Phys. Rev. D 50 (1994) 3614.
[18] Baesler S. et al., Improved test of the equivalence principle for gravitational self energy, Phys. Rev. Lett. V 83 (18) (1999).
[19] Dickey J.O. et al., Science 265 (1994) 482.
[20] Worden P. et al., Class. Quantum Grav. 13 (1996).
[21] Touboul P. et al., Class. Quantum Grav. 13 (1996).
[22] Nobili et al., The 'Galileo Galilei' (GG) project: testing the equivalence principle in space and on earth, in: Advances in Space Research, COSPAR, Nagoya, 1998.
[23] Everitt C.W.F. et al., SMEX Mission Selected for Study: STEP Satellite Test of Equivalence Principle, NASA, 2000.
[24] Nati M. et al., ASTRE a highly performant accelerometer for the low frequency range of the microgravity environment, in: 24th International Conference on Environment Systems Friedrichshafen, Germany, SAE, 1994.
[25] Touboul P., Foulon B., Le Clerc G., STAR the accelerometer of the geodesic mission CHAMP, IAF-98-B. 3.07, 1998.
[26] Touboul P. et al., Accelerometers for CHAMP, GRACE and GOCE, Bol. Geof. Teor. Ed. Appl. bg 090 (2000).
[27] Reigber C. et al., CHAMP mission status and perspectives, in: AGU Fall meeting, San Francisco, USA, 2000.
[28] GRACE: Science and Mission Requirements Document, revision A, JPL D-15928, 1998.
[29] Dittus H., Mehls C., A new experimental baseline for testing the weak equivalence principle at Bremen drop tower, Class. Quantum Grav. 18 (2001) 2417–2425.
[30] Marcuccio S. et al., FEEP Microthruster Technology Status and Potential Applications, AIAA, 1997.
[31] Fehringer M. et al., Micronewton indium thrusters, in: 26th International Electric Propulsion Conference, Kitakyushu, Japan, 1999.
[32] Gravity Field and Steady State Ocean Circulation Mission, ESA Publication SP-1233-1, 1999.
[33] Willemenot E., Touboul P., On-ground investigations of space accelerometers noise with an electrostatic torsion pendulum, Rev. Sci. Instrum. 71 (1) (2000) 302–309;
Willemenot E., Touboul P., Electrostatically suspended torsion pendulum, Rev. Sci. Instrum. 71 (1) (2000) 310–314.
[34] Josselin V., Touboul P., Kielbasa R., Capacitive detection scheme for space accelerometers applications, Sensors and Actuators A: Physical. 78 (1999) 92–98.
[35] Bonnet J. et al., Development of a thrust balance in the micro-newton range, in: 3rd International Conference Spacecraft Propulsion, Cannes, France, 2000.
[36] Josselin V., Rodrigues M., Touboul P., Inertial sensor concept for the gravity wave missions, Acta Astronautica 49 (2) (2001) 95–103.